J Intell Manuf (2007) 18:647–661
DOI 10.1007/s10845-007-0038-4

Finite element modeling of low speed reaming vibrations with reamer geometry modifications

S. Towfighian · K. Behdinan · M. Papini · Z. Saghir · P. Zalzal · J. de Beer

Received: June 2006 / Accepted: January 2007 / Published online: July 2007

Abstract Reaming is a finishing process used to remove a small amount of material from a predrilled hole. In low speed cutting processes, it is the formation of lobed or multi-cornered holes that is of concern, rather than tool chatter, which occurs at high speed near the natural frequency of the tool. Using a quasi-static model in the characteristic form for the reaming process, a finite element modeling for the low speed reaming process, based on the Euler–Bernoulli beam model, was developed. Cutting and rubbing forces were applied as concentrated and distributed forces on a variable engagement length of the reamer. The variable engagement length is considered to simulate the actual applied forces length as the reamer advances to the workpiece. The time dependant changes in the bending stiffness of the reamer were included in the governing equation of the equilibrium of the reamer, and its stability analysis was performed at different time steps. Using this model, the vibration damping effect of uneven spacing of reamer teeth was investigated. The results demonstrate that uneven spacing of reamer teeth reduces the tool vibration, and therefore leads to a more stable condition. Finally, the optimum configuration of uneven tooth pitch angles for a six-flute reamer, in order to have the highest vibration decay rate during the reaming, was presented.

Keywords Finite element model · Variable engagement length · Low speed reaming · Low frequency vibration · Hole profile · Irregular tooth spacing

S. Towfighian · K. Behdinan (✉)
Department of Aerospace Engineering,
Ryerson University,
Toronto, ON, Canada M5B 2K3
e-mail: kbehdina@ryerson.ca

M. Papini · Z. Saghir
Department of Mechanical and Industrial Engineering,
Ryerson University,
Toronto, ON, Canada M5B 2K3

P. Zalzal · J. de Beer
Orthopaedic Surgery Division, McMaster University,
Hamilton, ON, Canada

Introduction

Reaming is a cutting process used for enlarging and the precise sizing of predrilled holes. It is widely used in manufacturing processes as well as biomedical applications. Stability and hole quality during reaming is of great interest in the manufacturing process as it reduces fatigue, spindle wear, high loads and production cycles. An improvement in the hole quality can lead to a decrease in the process costs, and this has led to careful consideration of tool dynamics and vibration (Bayly, Lamar, & Calvert, 2002; Bayly, Metzler, Schaut, & Young, 2001b; Bayly, Young, Calvert, & Halley, 2001a; Bayly, Young, & Halley, 1998; Metzler, Bayly, Young, & Halley, 1999; Sakuma & Kiyota, 1968a,b).

Vibration leading to tool instability during reaming is divided into two categories: (1) regenerative chatter (self-excited) vibration and, (2) low frequency vibration (Bayly et al., 2002). In regenerative chatter, the vibration develops itself in subsequent revolutions through the generation of the waviness on the surface of the hole, and occurs when the tool rotates near its natural frequency under certain cutting conditions. In the low frequency vibration case, low speed cutting leads to the formation of multi-cornered profiles with periodicity.

Tool dynamics was initially investigated for turning and milling applications. Based on the concept of time-delayed

regenerative cutting forces causing chatter (Koenigsberger & Tlusty, 1970; Tlusty, 1985; Tlusty & Polacek, 1963; Tobias, 1965), the linear theory of chatter was introduced and the stability boundary predictions for turning and milling were discussed. A theoretical analysis of milling dynamics was subsequently conducted by Sridhar, Hohn, and Long (1968a, b). Sridhar developed a method to study the system's stability by examining the eigenvalues of the system's state transition matrix at one revolution period of the tool. Budak and Altintas (1993, 1995) later analytically predicted stability lobes for milling in a more accurate way.

A simplified model of the reamer which included cutting forces and rubbing forces on the clearance face and sides of the reamer was proposed by Young et al. (1998). Metzler et al. (1999) found analytical stability boundaries for drilling and reaming at high cutting speeds without process damping, by developing a general time-domain simulation. The drilling analysis was based on a boring model by Li, Ulsoy, and Endres (1998) and the reaming analysis was based on the method proposed for milling by Budak and Altintas (1998).

At low cutting speeds, reamer vibration is associated with tooth passing frequency, rather than the natural frequency in chatter. It causes the formation of a lobed-hole profile instead of a perfect hole. Low frequency vibration in reaming was experimentally investigated by Sakuma and Kiyota (1968a, 1968b). Their research showed that a deviation from the prebored hole axis and the manufacturing tolerances in tool margins resulted in multi-corner profiles. They observed that for reamers of N teeth, the numbers of lobes or corners in the hole profile would be $N+1$ or $N-1$.

Bayly et al. (2001a) introduced an analytical method to determine the fundamental solutions of the equations of motion for reaming at low cutting speed. They established a quasi-static model for reaming in which the inertia and damping forces were assumed negligible in comparison to the stiffness forces, and regenerative cutting forces as well as rubbing (friction) forces on the clearance faces were included. These forces were assumed as concentrated loads at the tip of the tool. The formulation led to an eigenvalue problem with solutions that included oscillatory and unstable modes.

In the present paper, finite element modeling is used to model the reaming process using the cutting and rubbing force formulation proposed by Bayly et al. (2001a). The finite element method is used to obtain an approximate solution for the continuous system of the reamer and to study the flexibility effect of the reamer on the vibrations. A new model of applying the loads on the tool is presented to make the simulations more realistic. Instead of a concentrated force at the reamer tip, we assume a uniform distributed force on a variable engagement length of the reamer which are tapered with small angles. This model thus includes the effect of the changing length over which the forces are applied while the reamer proceeds to the workpiece. Because the effective bending stiffness changes with time, a solution to the eigenvalue problem was sought at different time steps.

In order to improve the hole quality; i.e., avoiding the multi-cornered holes resulting from low frequency vibrations, both modifications to the reaming tool and the reaming process parameters can be made. We consider the former, by modifying the geometry of the reaming tool, in order to improve the stability, resulting in smoother holes. Irregular tooth spacing has been considered in the past as an effective method in reducing the roundness error (Bayly, 1997; Varterasian, 1974). In the present work, the effects of different orientations for irregular tooth spacing on resulting stability were compared. All possible orientations for a group of teeth spacing within an acceptable margin were compared, and the best combination for a six-flute reamer giving the most stable condition is presented.

As the rubbing coefficient depends on the particular properties of the two materials in contact, and has not been investigated in previous works, a range for rubbing coefficient was considered, and its effects on stability are presented for 2D and 3D hole profiles.

Process modeling

Reaming process modeling includes the modeling of both the reaming tool and the applied forces. The reaming tool was modeled as a cantilevered beam using Euler–Bernoulli beam elements, discussed in section "Finite element discretization." Cutting and rubbing force models described in sections "Cutting force model" and "Rubbing force model" are taken from the model proposed by Bayly et al. (2001a) for low cutting speeds up to 500 RPM on a 2D plane of cross section of the reamer.

The governing equation of equilibrium of the reamer leads to an eigenvalue problem that yields the frequency and nature of different modes of vibrations. For simplicity, we only consider each mode behavior separately for bending vibrations and neglect torsional vibrations. In addition, the model is quasi-static in the sense that inertia and damping are considered negligible compared to stiffness. Common terminology used for various parts of a reamer can be found in Fig.1.

Cutting force model

The cutting force in drilling operations was shown to be a function of chip load, as tested by drilling tubular aluminum specimens on a CNC vertical milling machine (Cincinnati Arrow 750) (Bayly et al., 2001b). A similar proportionality for reaming was proposed by Bayly et al. (2001a), and is used herein. In that assumption, the chip load was defined as the product of width of cut times feed per tooth.

Fig. 1 Reamer geometry

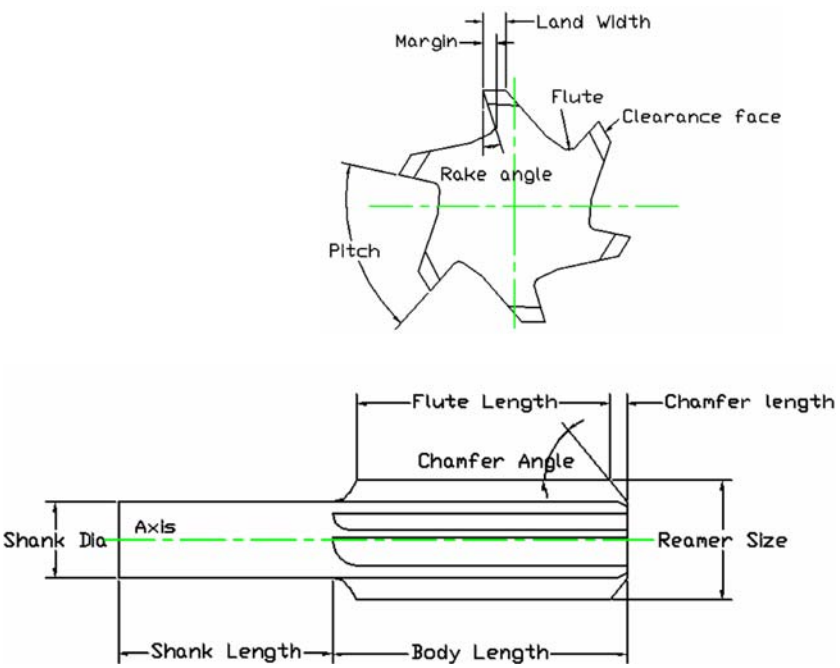

Fig. 2 Schematic diagram of the reaming process showing: (**a**) the nominal chip load (**b**) The effect of radial and axis tool displacement on chip load. The dotted line shows the chip area without displacement and the hatched area shows the chip area after tool displacement. Adapted from Bayly et al. (2001a)

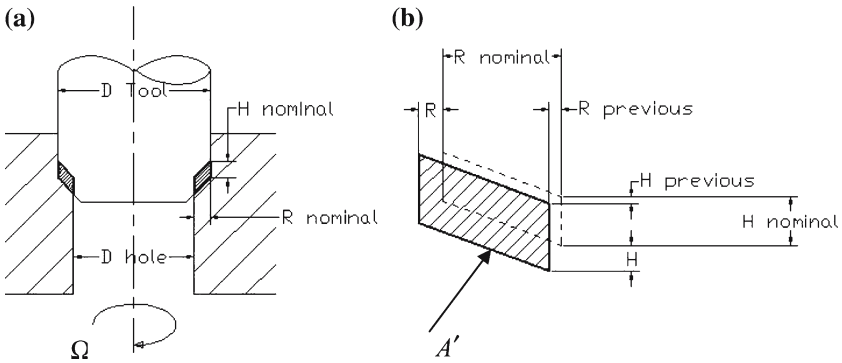

The chip load nominal area can be obtained from $A = H_{\text{nominal}} \times R_{\text{nominal}}$, where H_{nominal} is feed per tooth and R_{nominal} is width of cut (Fig. 2a). Vibration of the tool causes displacement of the tool with respect to the workpiece. Therefore, the nominal chip area changes to:

$$A' = (R_{\text{nominal}} + R - R_{\text{previous}}) \\ (H_{\text{nominal}} + H - H_{\text{previous}}) \quad (1)$$

where $R - R_{\text{previous}}$ is the radial and $H - H_{\text{previous}}$ is the vertical displacement of the tool center (Fig. 2b). For small deflections and a typical reamer chamfer angle of 45° ($R - R_{\text{previous}} = H - H_{\text{previous}}$), the change in the chip area can be written as:

$$\Delta A = A' - A = (R_{\text{nominal}} + H_{\text{nominal}})(R - R_{\text{previous}}) \quad (2)$$

The difference in cutting force can be assumed to be roughly a linear function of changes in radial depth of cut:

$$\Delta F = k_c(R - R_{\text{previous}}) \quad (3)$$

where $k_c = k_s(R_{\text{nominal}} + H_{\text{nominal}})$ is the cutting coefficient or stiffness, and k_s is the specific cutting pressure for different materials.

The coordinate system chosen is the $x - y$ system, which rotates at the tool speed of Ω with its center fixed at the center of the hole (Fig. 3b). As this axis system is parallel to the $x'-y'$ system (i.e., the local axis attached to the reamer rotating with Ω), the components of the cutting force difference in both axes are the same. Therefore, the components of the cutting force difference on each tooth (Fig. 3a) can be written as:

$$F_{cx}^{(i)} = k_c\left[R_i(t) - R_{i+1}(t - \tau_i)\right]\cos\left(\phi_i - \frac{\pi}{2} - \alpha\right) \quad (4a)$$

$$F_{cy}^{(i)} = k_c\left[R_i(t) - R_{i+1}(t - \tau_i)\right]\sin\left(\phi_i - \frac{\pi}{2} - \alpha\right) \quad (4b)$$

where $R_i(t)$ is the radial depth of cut for the ith tooth at the time t and $R_{i+1}(t - \tau_i)$ is the radial depth of cut for the proceeding tooth at the time $t - \tau_i$, and $\tau_i = \frac{(\phi_{i+1} - \phi_i)}{2\pi} \cdot T$ is

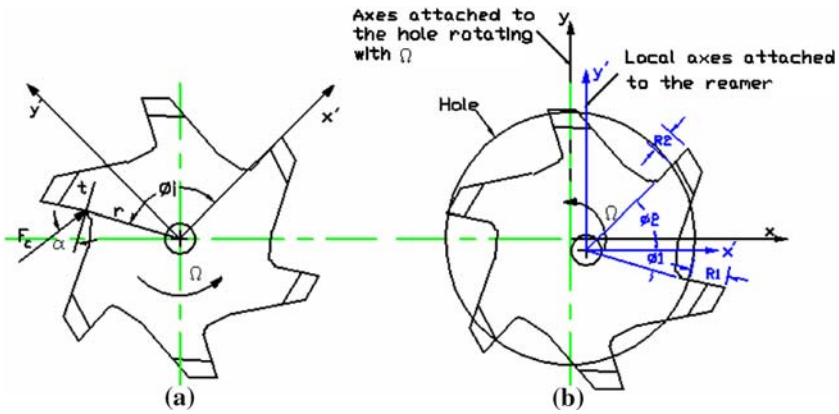

Fig. 3 (**a**) Cutting forces acting on the tool (**b**) Tool axis motion and radial displacement of each tooth

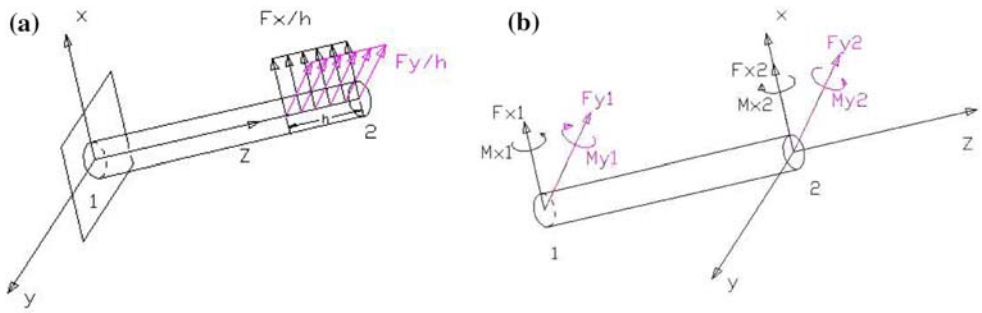

Fig. 4 (**a**) Distributed forces on reamer as a cantilever beam. (**b**) Distributed forces replacement

the period between successive tooth engagements. The angle between the total cutting force direction and the direction tangent to the tool is the cutting angle, α, and is assumed constant during cutting.

The radial position of each tooth can be written in terms of displacement of the center.

$$R_i(t) = \cos\phi_i x(t) + \sin\phi_i y(t) \tag{5}$$

When the time is normalized; then $\tau_i = \tau_0 = \frac{2\pi}{N}$ for an even spacing of teeth. Substituting Eq. 5 into Eqs. 4a and 4b, and adding the forces for all teeth, the total cutting force in the case of even spacing of teeth is

$$\begin{bmatrix} F_{cx} \\ F_{cy} \end{bmatrix} = K_{c0} \begin{bmatrix} x(t) \\ y(t) \end{bmatrix} - K_{cN} \begin{bmatrix} x(t-\tau_0) \\ y(t-\tau_0) \end{bmatrix} \tag{6}$$

where

$$K_{cN} = k_c \sum_{i=1}^{N} \begin{bmatrix} C_i c_{i+1} & C_i s_{i+1} \\ S_i c_{i+1} & S_i s_{i+1} \end{bmatrix} \tag{7}$$

$$K_{c0} = k_c \sum_{i=1}^{N} \begin{bmatrix} C_i c_i & C_i s_i \\ S_i c_{i1} & S_i s_i \end{bmatrix} \tag{8}$$

with $c_i = \cos\phi_i$, $s_i = \sin\phi_i$, $C_i = \cos(\phi_i - \frac{\pi}{2} - \alpha)$, and $S_i = \sin(\phi_i - \frac{\pi}{2} - \alpha)$.

For a generalized spacing of teeth, $\tau_i = \phi_{i+1} - \phi_i$, and the total cutting force in vector form becomes

$$\vec{F}_c = \begin{bmatrix} F_{cx} \\ F_{cy} \end{bmatrix} = K_{c0} \begin{bmatrix} x(t) \\ y(t) \end{bmatrix} - \sum_{i=1}^{N} K_{ci} \begin{bmatrix} x(t-\tau_i) \\ y(t-\tau_i) \end{bmatrix} \tag{9}$$

where

$$K_{ci} = k_c \begin{bmatrix} C_i c_{i+1} & C_i s_{i+1} \\ S_i c_{i+1} & S_i s_{i+1} \end{bmatrix} \tag{10}$$

Rubbing force model

The reamer rubbing force is a force on the cutting edge caused by rubbing against the newly removed material. This force has tangential as well as radial components, the main portion of which is applied at the clearance face of the reamer (Bayly et al., 2001b). It can be formulated in a manner similar to the cutting force:

$$\vec{F}_r = \begin{bmatrix} F_{rx} \\ F_{ry} \end{bmatrix} = K_r \begin{bmatrix} x(t) \\ y(t) \end{bmatrix} - K_r \begin{bmatrix} x(t-\tau_r) \\ y(t-\tau_r) \end{bmatrix} \tag{11}$$

where:

$$K_r = k_r \sum_{i=1}^{N} \begin{bmatrix} C_{ri} c_i & C_{ri} s_i \\ S_{ri} c_{i1} & S_{ri} s_i \end{bmatrix} \tag{12}$$

Table 1 Experimental data from Bayly et al. (2001a)

	Material	Aluminum
Reamer specifications:		
N	Number of teeth	6
Ω	Spindle speed	250 RPM
L_0	Length of the reamer	159 mm
d	Diameter of the reamer	12.7 mm
k_s	Specific cutting pressure	2.4×10^3 N/mm^2
f	Feed	0.152 mm/rev
R_{nominal}	Width of cut	0.254 mm
H_{nominal}	Feed per tooth	0.25 mm/rev
k_c	Cutting stiffness	663 N/mm
k_r	Rubbing stiffness	0.211–211 N/mm
$k_{xx} = k_{yy}$	Bending stiffness for the one element model and concentrated force where $K = \begin{bmatrix} k_{xx} & 0 \\ 0 & k_{yy} \end{bmatrix}$	16.9 N/mm
μ	Friction coefficient	0.2
α	Cutting angle	$\frac{\pi}{6}$
θ_r	Angular width of radial margin	2 degrees

$$C_{ri} = \cos\left(\phi_i - \frac{\pi}{2} - \beta\right), S_{ri} = \sin\left(\phi_i - \frac{\pi}{2} - \beta\right), \quad c_i = \cos\phi_i, s_i = \sin\phi_i \tag{13}$$

and $\tau_r = \frac{\theta_r}{2\pi} \cdot T$. θ_r is the angular width of radial margin, and k_r is the rubbing coefficient. The friction angle, $\beta = \arctan\mu$, where μ is the coefficient of friction.

Finite element discretization

In order to study the deformation of the reamer which is a continuous system caused by cutting and rubbing forces, the reamer was divided into a number of elements lengthwise, based on the Euler–Bernoulli beam model. This model assumes a small ratio of depth to length of the beam (<0.1) and negligible shear deformation and rotary inertia. Finite element modeling was used to consider the flexibility of the reamer on vibrations and to approximate a solution for the continuous system of the reamer. First the reamer was modeled as a cantilevered beam with one element and its behavior was studied under concentrated and distributed forces. Subsequently, a similar analysis was performed on the reamer using more elements.

The concentrated force model

For the one element model of the reamer, cutting and rubbing forces were applied as concentrated nodal forces at the reamer tip. The first node was fixed and the second node was the tool tip. The dependence of the bending force on the tool center displacements and rotations was assumed to be linear. Each node has four degrees of freedom: displacements in the x and y direction, and rotations about the $x-y$ axis. Imposing the boundary conditions of a cantilever beam yields:

$$\frac{EI}{L^3}\begin{bmatrix} 12 & 0 & 0 & -6L \\ 0 & 12 & 6L & 0 \\ 0 & 6L & 4L^2 & 0 \\ -6L & 0 & 0 & 4L^2 \end{bmatrix}\begin{Bmatrix} u_2 \\ v_2 \\ \phi_{2u} \\ \phi_{2v} \end{Bmatrix} = \begin{Bmatrix} F_{x2} \\ F_{y2} \\ M_{x2} \\ M_{y2} \end{Bmatrix} = \begin{Bmatrix} F_x \\ F_y \\ 0 \\ 0 \end{Bmatrix} \tag{14}$$

F_x, F_y are concentrated forces applied at node 2 (the tool tip), defined as

$$F_x = -(F_{cx} + F_{rx}) \tag{15}$$

$$F_y = -(F_{cy} + F_{ry}) \tag{16}$$

where F_{cx}, F_{cy} and F_{rx}, F_{ry} are the cutting and rubbing force components in the x and y directions, respectively. The corresponding Eqs. 9 and 11 are substituted into Eqs. 15 and 16 and, subsequently into Eq. 14. Simplifying the resulting equation, solving for u_2, v_2, and setting $u_2 = x(t)$, $v_2 = y(t)$, gives:

$$\frac{EI}{L^3}\begin{bmatrix} 3 & 0 \\ 0 & 3 \end{bmatrix}\begin{Bmatrix} x(t) \\ y(t) \end{Bmatrix} = \begin{Bmatrix} F_x \\ F_y \end{Bmatrix} = \vec{F}_B \tag{17}$$

where EI is the flexural rigidity of the reamer material and L is the length of the beam element. Therefore, the bending stiffness matrix for the concentrated force model can be written as:

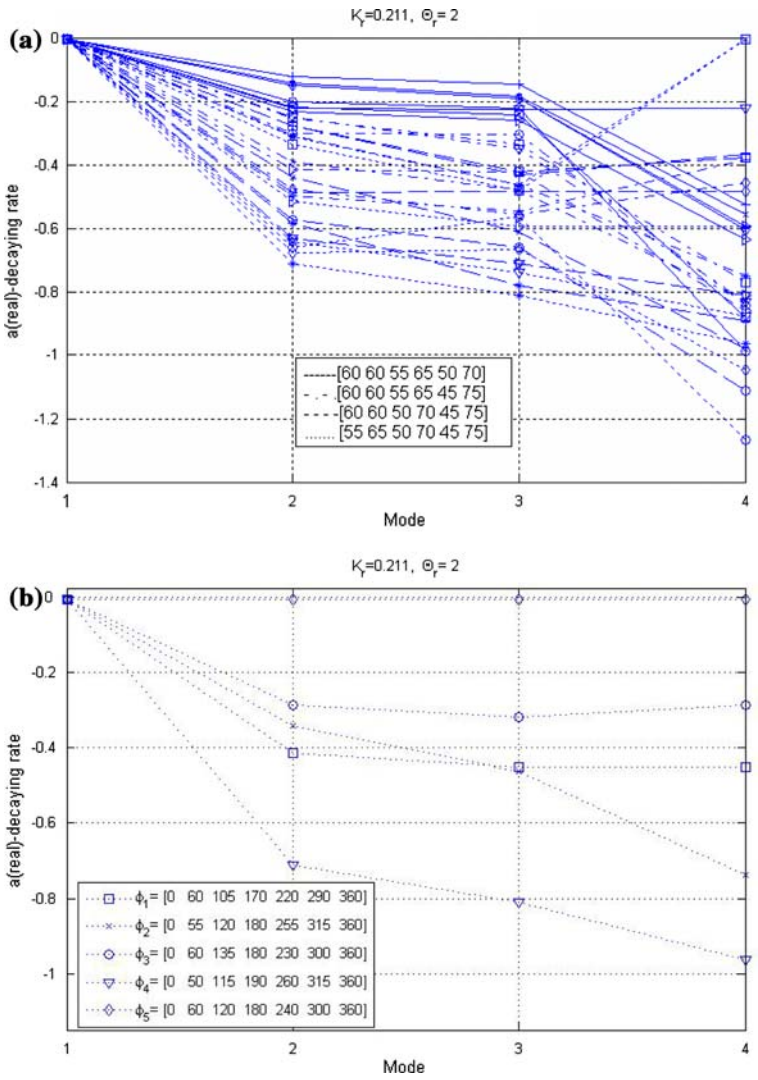

Fig. 5 Real part values of four modes for (**a**) 32 different orientations of teeth in four groups (**b**) five different orientations (b = 1 in Mode1, b = 5 in Mode2, b = 7 in Mode3 and b = 11 in Mode4)

$$K = \frac{EI}{L^3}\begin{bmatrix} 3 & 0 \\ 0 & 3 \end{bmatrix} \tag{18}$$

For the multi-element beam model, the first node is fixed and other nodes are numbered toward the tool tip. Similar to the one element model, the concentrated rubbing and cutting forces are applied at the tool tip. After imposing the boundary conditions and solving the resulting equation for the $x(t)$, $y(t)$ displacements of the node at the reamer tip, an identical relation to Eq. 18 is obtained.

The distributed force model

The use of a distributed force along the reamer length is considered to make the simulation of the process closer to the real situation. This is because commonly used reamers that are tapered with an angle at least 0.5 degrees result in forces being applied on the reamer not only at the tip, but also along the engagement length of the reamer. In the present work, a distribution of applied forces on the reamer was assumed along the engagement length, rather than a concentrated force on the tool tip. The force distribution was assumed uniform for simplicity, but other forms of the force distribution yielding higher forces at the tool tip are also feasible. Thus, for the one element model of the reamer, cutting and rubbing forces are applied as a uniform distributed forces along the engagement length, h, measured from the tool tip (Fig. 4a). As the reamer advances, the engagement length changes with time $h(t) = \frac{f \cdot \Omega}{60} \cdot t$, where f is the feed, Ω is the spindle speed, and t is the time. In this scheme, distributed forces are replaced by nodal forces (Fig. 4b). Using Euler–Bernoulli beam theory, the displacement of the beam in $x-z$ and $y-z$ planes can be represented by a cubic function of z along the length of the reamer (Cheung & Leung, 1991). Therefore, the nodal force replacements of distributed forces were derived from Logan (1999), as

Table 2 Real part of eigenvalues, a, for tooth spacing orientations yielding the minimum values for each of the first four modes

Pitch angle combinations (°)	Min for mode	Mode1 (b=1)	Mode2 (b=5)	Mode3 (b=7)	Mode4 (b=11)
ϕ = [0 70 145 210 255 310]	1	−0.0041	−0.6776	−0.6750	−1.1668
ϕ = [0 45 95 160 235 305]	2	−0.0041	−0.7115	−0.8108	−0.9625
ϕ = [0 45 95 160 215 290]	3	−0.0041	−0.4780	−0.8763	−0.7288
ϕ = [0 50 125 180 245 290]	4	−0.0041	−0.6645	−0.5716	−1.5020

Table 3 Frequency values b (imaginary part of eigenvalue) and associated type of vibration (Backward; $d = -1$, Forward ; $d = 1$)

Values	Mode1	Mode2	Mode3	Mode4
Frequency (cyc/rev)	1	5	7	11
Type	Backward	Forward	Backward	Forward

Table 4 Real part of eigenvalue, a for $k_r = 0.211$ N/mm in concentrated force case for regular and irregular spacing of teeth

Regular spacing				Irregular spacing			
Mode1 (b=1)	Mode2 (b=5)	Mode3 (b=7)	Mode4 (b=11)	Mode1 (b=1)	Mode2 (b=5)	Mode3 (b=7)	Mode4 (b=11)
−0.0041	−0.0041	−0.0040	−0.0042	−0.0041	−0.7115	−0.8108	−0.9625

Table 5 Real part of eigenvalue, a for $k_r = 211$ N/mm in concentrated force case for regular and irregular spacing of teeth

Regular spacing				Irregular spacing			
Mode1 (b=1)	Mode2 (b=5)	Mode3 (b=7)	Mode4 (b=11)	Mode1 (b=1)	Mode2 (b=5)	Mode3 (b=7)	Mode4 (b=11)
0.0020	−0.0383	0.0297	−0.0868	0.0020	−0.7258	−0.7639	−0.9392

$$\{Q\} = \int_{l-h}^{l} [N]^T \{P\}\, dz \tag{19}$$

where $\{Q\} = \left\{F_{x1}, F_{y1}, M_{x1}, M_{y1}, F_{x2}, F_{y2}, M_{x2}, M_{y2}\right\}^T$, and $[N]$ is the shape function. The uniformly distributed force is:

$$\{P\} = \begin{Bmatrix} P_x \\ P_y \end{Bmatrix} = \frac{1}{h\,(t)} \begin{Bmatrix} F_x \\ F_y \end{Bmatrix} \tag{20}$$

where F_x and F_y are as in Eqs. 15 and 16. The force replacement vector of the tool tip is related to the displacements and rotations of that point by the stiffness matrix. Therefore, the relation between external forces (F_x, F_y) and nodal displacements of the tip becomes:

$$EI \begin{bmatrix} \frac{24}{h^3(t)+8L^3-6L^2h(t)} & 0 \\ 0 & \frac{24}{7h^3(t)+8L^3+6L^2h(t)-16Lh^2(t)} \end{bmatrix} \times \begin{Bmatrix} x(t) \\ y(t) \end{Bmatrix} = \begin{Bmatrix} F_x \\ F_y \end{Bmatrix} \tag{21}$$

Consequently, the revised bending stiffness matrix for the distributed force model on the variable engagement length of the reamer for the one element model is written as:

$$K\,(t) = EI \begin{bmatrix} \frac{24}{h^3(t)+8L^3-6L^2h(t)} & 0 \\ 0 & \frac{24}{7h^3(t)+8L^3+6L^2h(t)-16Lh^2(t)} \end{bmatrix} \tag{22}$$

where $h(t)$ is the length of applied forces that changes with time, and L is the length of the beam element.

For the multi-element model of the reamer, the revised bending stiffness is obtained after assembling the stiffness and force replacement matrices, imposing the boundary conditions, and solving for the last node displacements. The stiffness matrix derived in the same manner as in Eq. 22, will be used in the equilibrium equations that follow.

Equilibrium equations and solution

Regarding the assumptions made to get the quasi-static model, the equilibrium of forces in a plane normal to the axis of the tool is written as $\vec{F}_B + \vec{F}_c + \vec{F}_r = 0$.

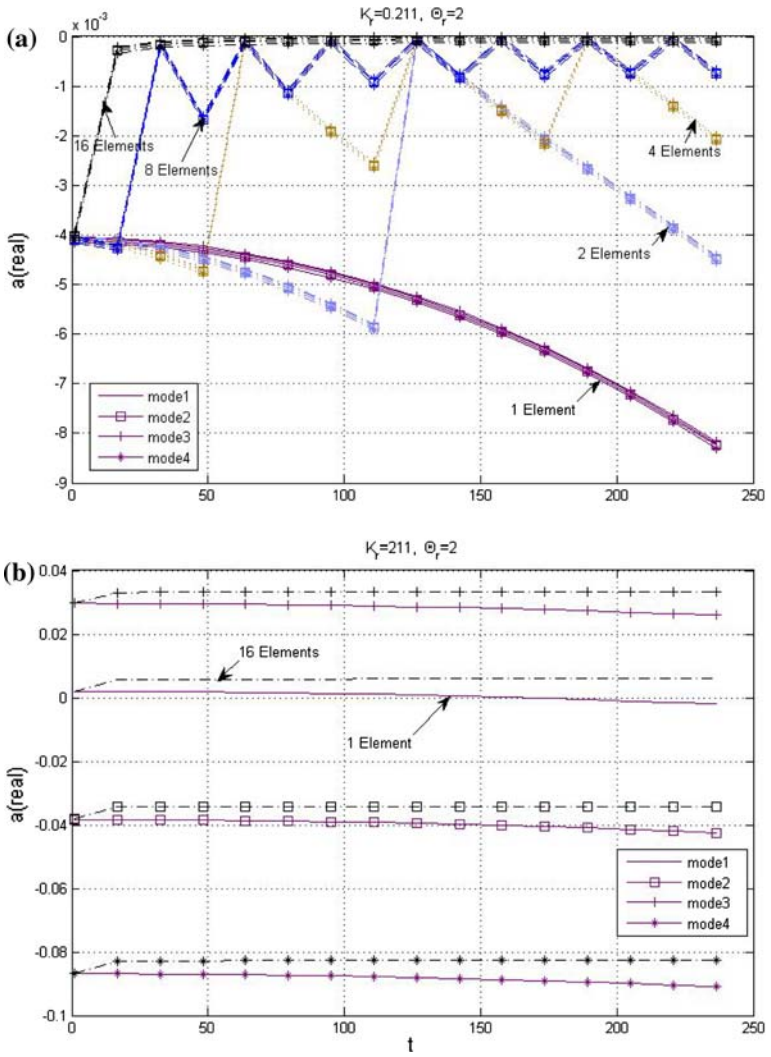

Fig. 6 Results for eigenvalues, a in $x(t) = Aue^{(a+ib)t}$ versus time for variable engagement length case for applied force, when regular spacing of teeth, $\theta_r = 2$ degrees and (**a**) $k_r = 0.211$ (**b**) $k_r = 211$ (1 element: solid line, 2 elements: dash-dot line and 4 elements: dotted line)

For general spacing, replacing $\vec{F}_B$, $\vec{F}_c$ and $\vec{F}_r$ from Eqs. 17, 9 and 11, respectively, yields (Bayly et al., 2001)

$$K\vec{x} + K_{c0}\vec{x} - \sum_{i=1}^{N} K_{ci}\vec{x}(t-\tau_i) + K_r\left[\vec{x} - \vec{x}(t-\tau_r)\right] = 0 \tag{23}$$

For even spacing, replacing $\vec{F}_B$, $\vec{F}_c$ and $\vec{F}_r$ from Eqs. 17, 6 and 11, respectively, giving (Bayly et al., 2001):

$$K\vec{x} + K_{c0}\vec{x} - K_{cN}\vec{x}(t-\tau_0) + K_r\left[\vec{x} - \vec{x}(t-\tau_r)\right] = 0 \tag{24}$$

To solve this equation, $\vec{x}$ is replaced in the characteristic form ($\vec{x} = A\vec{u}e^{\lambda t}$), and an eigenvalue equation is obtained as follows (Bayly et al., 2001):

$$\left\lfloor K + K_{c0} - K_{cN}e^{-\lambda\tau_0} + K_r\left(1 - e^{-\lambda\tau_r}\right)\right\rfloor A\vec{u}e^{\lambda t} = 0 \tag{25}$$

where $\lambda = a + ib$ is the eigenvalue and $\vec{u} = \begin{bmatrix} c+id \\ 1 \end{bmatrix}$ is the eigenvector. The imaginary part of λ shows the frequency of oscillation, and the real part describes the growth or decay rate. The value of A, the amplitude of a specific mode, is determined by the initial conditions in the experiments.

Equation 25 has a non-trivial solution only if the determinant of the matrix on the left-hand side is set to zero (Bayly et al., 2001):

$$\det\left\lfloor K + K_{c0} - K_{cN}e^{-(a+ib)\tau_0} + K_r\left(1 - e^{-(a+ib)\tau_r}\right)\right\rfloor = 0 \tag{26}$$

This equation shows the eigenvalue equation for even spacing. A similar equation can be derived for general spacing (Bayly et al., 2001):

$$\det\left[K + K_{c0} - \sum_{i=1}^{N} K_{ci}e^{-(a+ib)\tau_i} + K_r\left(1 - e^{-(a+ib)\tau_r}\right)\right] = 0 \tag{27}$$

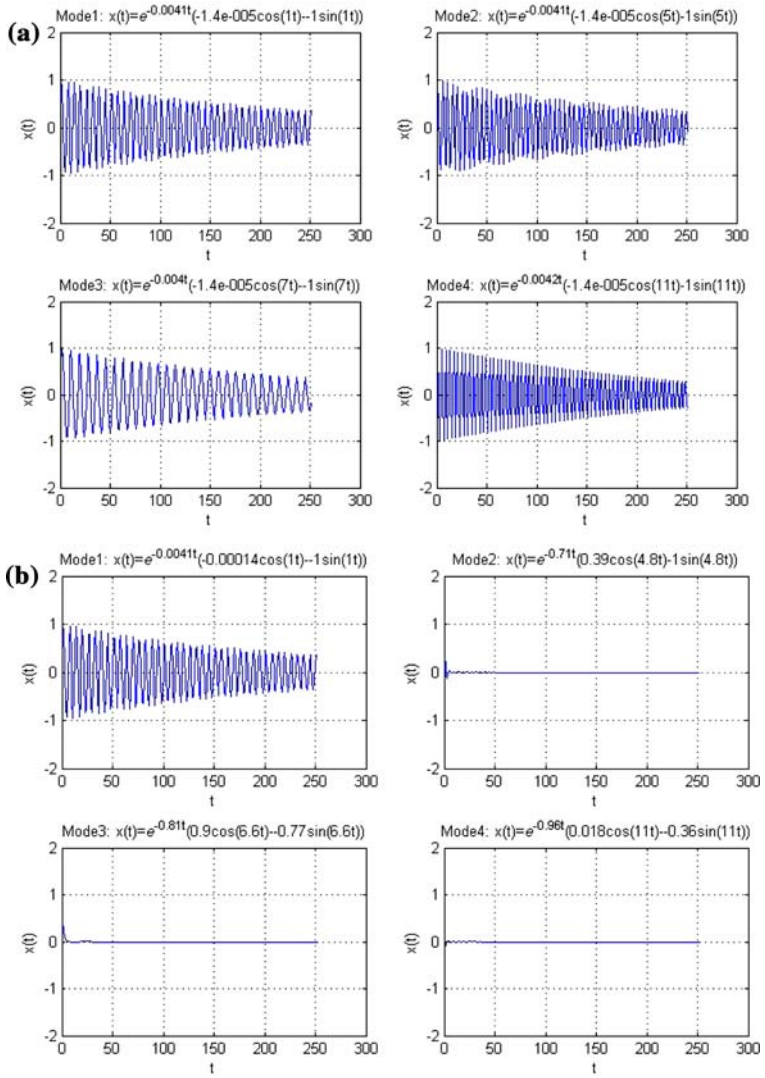

Fig. 7 Displacement of the tool axis in the x direction versus time for the concentrated force model ($k_r = 0.211$ N/mm, $\theta_r = 2$ degrees, $\alpha = \frac{\pi}{6}$). (**a**) Regular (**b**) Irregular spacing

Equations 26 and 27 are non-linear systems of equations, including imaginary and real parts, which must be solved for a and b, the real and imaginary parts of λ, respectively. In these equations, K_{cN}, K_{c0}, K_{ci} and K_r are replaced from Eqs. 7, 8, 10 and 12, respectively, and the bending stiffness, K is substituted from Eq. 18, for the case of the concentrated force. For the distributed force model, the bending stiffness, K is substituted from Eq. 22 at a specific time $t = t_0$, and Eqs. 26 and 27 are rewritten for even spacing as:

$$\det\left[K(t_0)+K_{c0}-K_{cN}e^{-(a+ib)\tau_0}+K_r\left(1-e^{-(a+ib)\tau_r}\right)\right]=0 \tag{28}$$

and for general spacing as:

$$\det\left[K(t_0)+K_{c0}-\sum_{i=1}^{N}K_{ci}e^{-(a+ib)\tau_i} +K_r\left(1-e^{-(a+ib)\tau_r}\right)\right]=0 \tag{29}$$

These equations were solved for a and b at $t_0 = \left[0, \frac{60\cdot L_0}{f\cdot\Omega}\right]$, where L_0 is the length of the reamer and $\frac{60\cdot L_0}{f\cdot\Omega}$ is the time when the reamer reaches its end. With a and b determined, λ is known and the eigenvector $\vec{u} = \begin{bmatrix} c+id \\ 1 \end{bmatrix}$ can be obtained by solving Eq. 25 for even spacing in the concentrated force model, and in similar equations for the other cases. Finally, the axis tool vibration for each mode can be written as Bayly et al. (2001a):

$$\vec{x} = \begin{bmatrix} x(t) \\ y(t) \end{bmatrix} = Ae^{at}\begin{bmatrix} c\cos bt - d\sin bt \\ \cos bt \end{bmatrix} \tag{30}$$

Illustrative example and discussion

In this section, the stability of vibration and 2D and 3D hole profiles is discussed for two different force models and different types of pitch spacing. The data used in this example

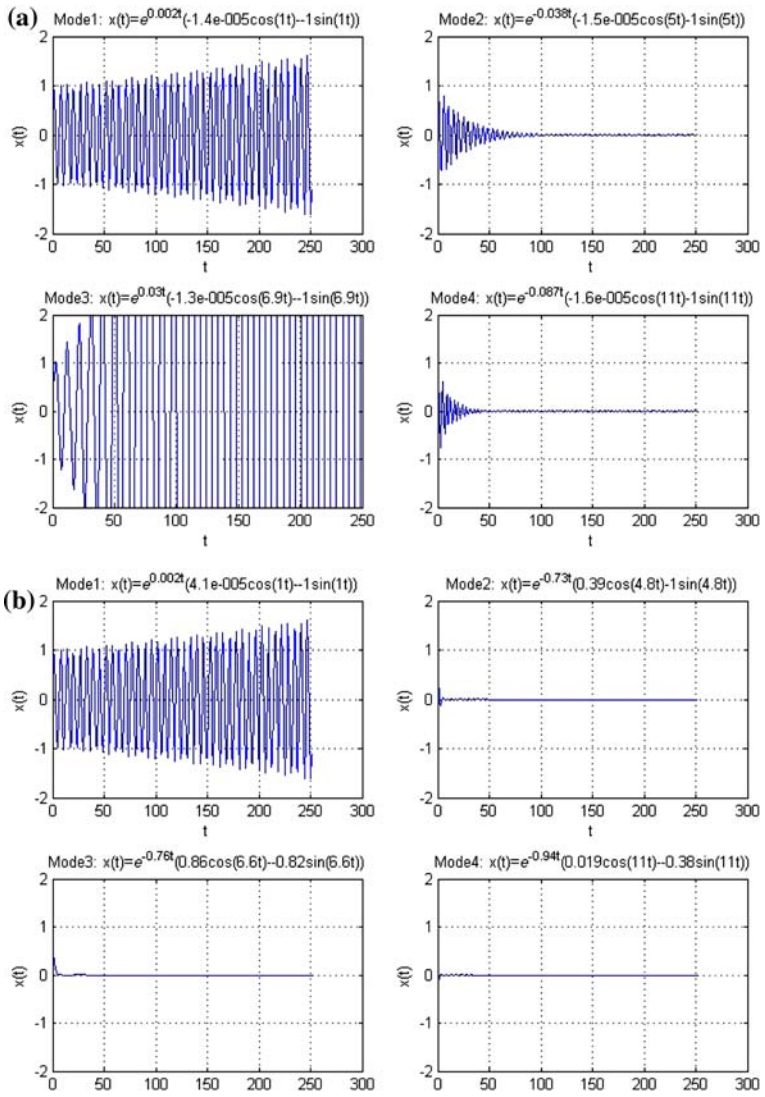

Fig. 8 Displacement of the tool axis in the x direction versus time for the concentrated force model ($k_r = 211\,\text{N/mm}$, $\theta_r = 2$ degrees, $\alpha = \frac{\pi}{6}$). (**a**) Regular (**b**) Irregular spacing

are from the reaming of aluminum in the aircraft industry (Bayly et al., 2001), and are summarized in Table 1. Regarding the model of forces and type of tooth spacing, the appropriate one of the equations of 26–29 was solved for eigenvalues using the Newton–Raphson iteration method and subsequently eigenvectors were sought. Results were obtained for two cases of regular/irregular placement of teeth and for two assumptions of forces applied on the reamer:

1. Concentrated nodal forces on the tip of the tool
2. Distributed forces on variable engagement length of the reamer.

The vibrations of first four modes are considered here because of their importance. All modes are expected to be present and the prevalence of each mode is determined by the initial conditions and the rate of decay or growth. Here each mode behavior is considered separately for simplicity.

Regular and irregular spacing of teeth

In previous investigations (Bayly, 1997; Varterasian, 1974), uneven tooth spacing has been introduced as an effective way to reduce vibrations. Here, combinations of irregular tooth angles for a six-flute reamer in a range of 5–15 degrees deviation from even spacing, with 5 degree increment and decrements, is investigated below. For more details one can refer to Towfighian (2006).

To determine the best tooth placement which yields the most negative real part of the eigenvalue, λ, 32 combinations of tooth angular positions based on the four groups of tooth spacing listed below were considered:

1 – [60 60 55 65 50 70]
2 – [60 60 55 65 45 75]
3 – [60 60 50 70 45 75]
4 – [55 65 50 70 45 75]

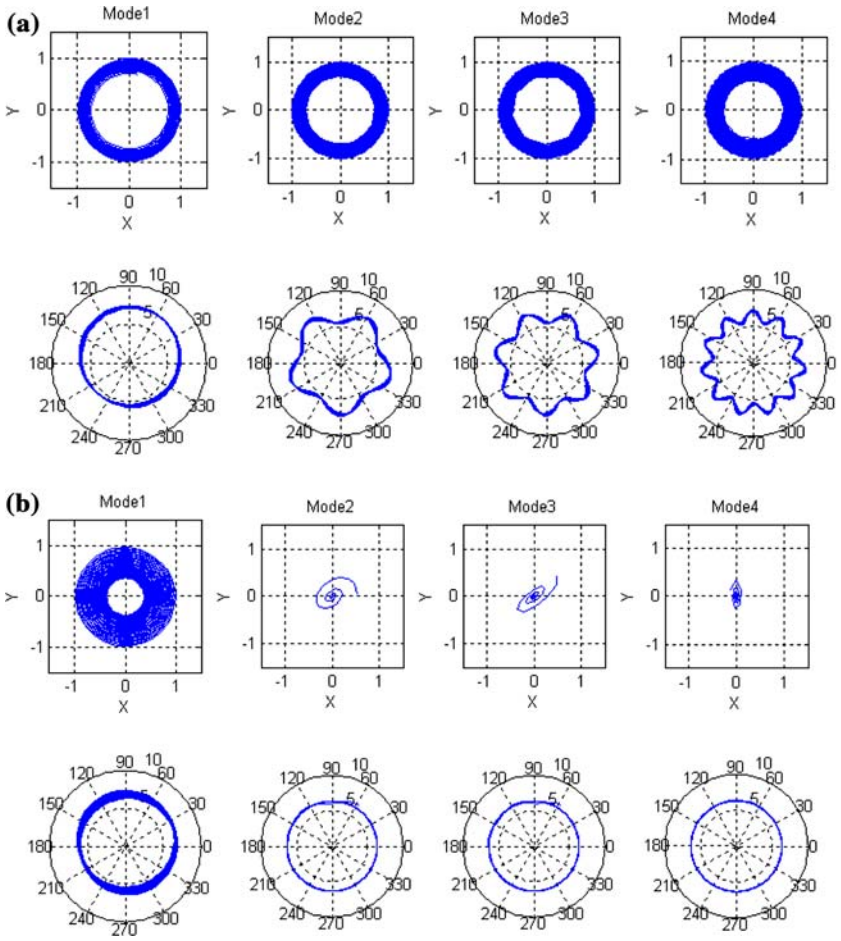

Fig. 9 Tool Axis trajectory and hole profiles for the distributed force model on the variable engagement length for 16 elements ($k_r = 0.211$ N/mm, $\theta_r = 2$ degrees, $\alpha = \frac{\pi}{6}$). (**a**) Regular (**b**) Irregular spacing

Eigenvalue results are shown for the case of concentrated force; for each group of angles, eight sets of orientations were considered (Fig. 5a). Each group is shown with a specific line style and different placements are shown with different markers. The comparison between four different placements, each from a spacing group of Fig. 5a and even spacing, is shown in Fig. 5b. As can be seen, in the case of even spacing, a, the real part of the eigenvalue, λ, is near zero, which shows periodic motion. In contrast, uneven pitch spacing results in negative values or damping vibrations.

Among the groups shown in Fig. 5a and b, the fourth group appears to give the highest decaying rate values. Therefore, for the fourth group of pitch spacing ([55 65 50 70 45 75]), 720 different possible orientations in a circle were considered and those that yielded the smallest real part value for each mode are listed in Table 2. Among the orientations in Table 2, the second orientation [0 45 95 160 235 305] that gives values closest to minimum for all modes has been chosen for the irregular tooth spacing in the following results.

Stability analysis

The stability analysis was performed by obtaining the eigenvalue and eigenvectors. For the case of the forces being concentrated forces at the tip of the reamer, values for a (real part of the eigenvalue) for the first four modes are given in Tables 4 and 5, and values for eigenvalue b (imaginary part) and eigenvector d are shown in Table 3. In all cases, the eigenvector c equals zero (Eq. 27). The results are listed for the one element model because in the case of a concentrated force, the reduced bending stiffness is the same regardless of the number of elements (Eq. 18).

Eigenvalue and eigenvector results are shown in Tables 4 and 5 based on two rubbing coefficients proposed by Bayly et al. (2001a). In regular spacing, increasing the rubbing coefficient k_r causes instability in the first and third modes and stability in the second and fourth modes. For the irregular case, it causes more stability only in the second mode of vibration. Irregular spacing in both values of k_r, in comparison to the regular case, resulted in higher damped vibrations

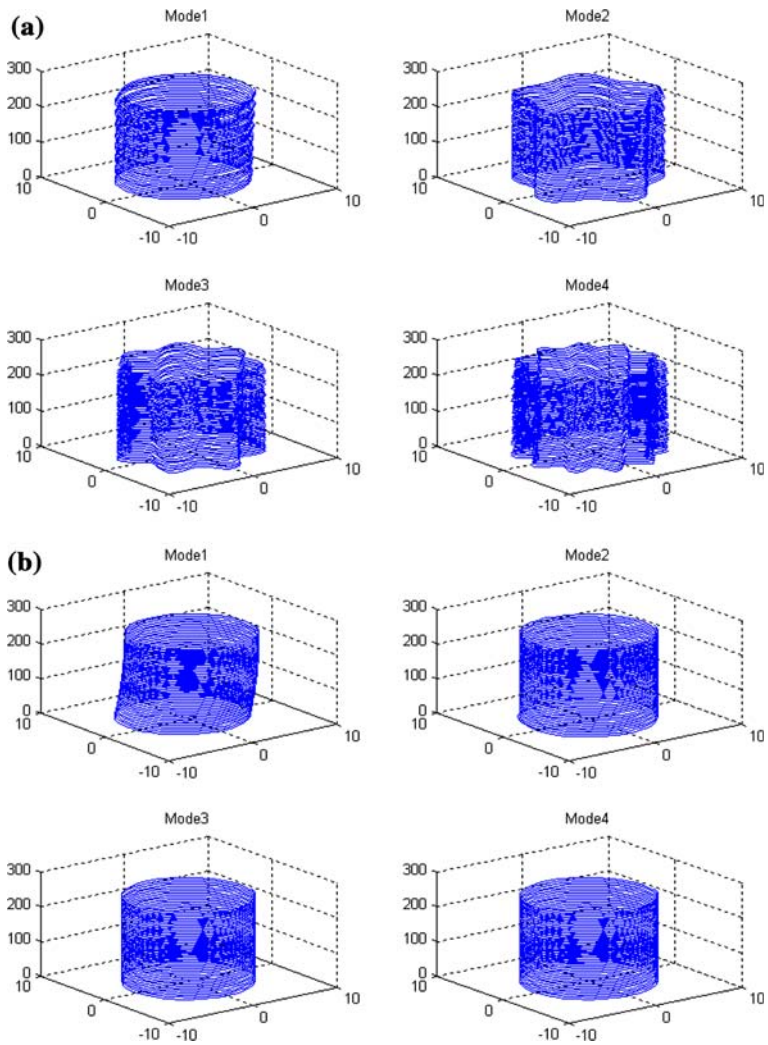

Fig. 10 3D hole profiles for the distributed force model on the variable engagement length for 16 elements ($k_r = 0.211$ N/mm, $\theta_r = 2$ degrees, $\alpha = \frac{\pi}{6}$). (**a**) Regular (**b**) Irregular spacing

for all modes other than one, although it did not change the vibration mode 1 (Tables 4, 5).

In practice, the applied force on the reamer is a distributed force on a length that increases as the reamer advances. The second assumption for the forces is therefore that the forces are distributed on a variable engagement length, as discussed in section "The distributed force model."

The revised stiffness matrix is given in Eq. 22 for one element, and in the multi-element model, the stiffness matrix is derived in the same way. Equations 28 and 29 were solved for the eigenvalues and subsequently the eigenvectors were obtained for the time interval of $t_0 = \left[0, \frac{60 \cdot L_0}{f \cdot \Omega}\right]$. Results of the decaying rate variations with time are shown in Fig. 6a and b, for the first four modes and two different rubbing coefficients. It is noted that the imaginary part of eigenvalue or frequency remains unchanged over time.

As depicted in Fig. 6a, for small rubbing coefficient systems, the real part value shows large variations with time. At $t = 0$, the decaying rate equals that of the concentrated force model, which has been used to date in the literature. For multi-element models (e.g., the 16 element model), the real part value starts from a negative value for concentrated force, approaching zero and showing a periodic motion as the time and number of elements increase. Models up to 16 elements are shown because the results converged at this number of elements. Figure 6a demonstrates that the concentrated force model yields very conservative eigenvalue results in comparison to the distributed force model. With the concentrated force model, tool vibration is completely damped while in the distributed force model, tool vibration starts from a damped vibration but becomes periodic as time passes and the reamer proceeds. In Fig. 6b, by increasing the rubbing coefficient, the real part shows a small variation with time for the first four modes. Furthermore, the difference in results for different numbers of elements is not large. This shows that for high values of rubbing coefficient, the assumption of concentrated force yields very close results to those of the distributed force model.

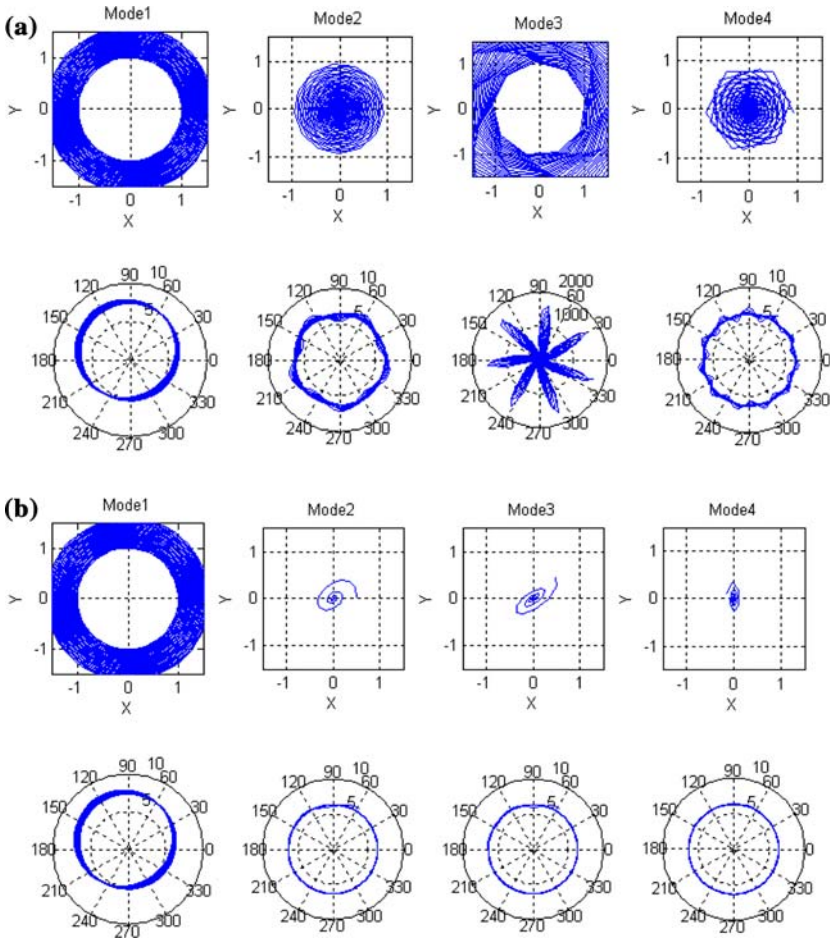

Fig. 11 Tool Axis trajectory and hole profiles for the distributed force model on the variable engagement length for 16 elements ($k_r = 211$ N/mm, $\theta_r = 2$ degrees, $\alpha = \frac{\pi}{6}$). (**a**) Regular (**b**) Irregular spacing

To study the effect of tooth spacing, time series graphs are shown in Figs. 7 and 8 for two different rubbing coefficients. They are depicted based on the results listed in Tables 4 and 5. Stability effects of irregular spacing on modes 2–4 can be seen from Figs. 7 and 8, although it did not change the first mode of vibration.

2D and 3D hole profiles

In order to obtain the hole profiles and axis trajectories, the 16 element beam model with distributed forces on variable engagement length was used for more accurate results. Hole profiles and tool axis trajectories for regular and irregular spacing are shown in Figs.9 and 11 for two k_r and 3D profiles in Figs. 10 and 12. As presented, the frequency of tool oscillation listed in Table 3 is associated with the number of lobed holes in Figs. 9–11.

The positive effect of irregular spacing of teeth on disappearance of lobed holes is depicted in Figs.9 and 11. 3D profiles of even spacing can be seen in Figs. 10a and 12a, and uneven spacing in Figs. 10b and 12b. Figures 10b and 12b show the 3D profile of the hole which is very close to the perfect hole. The close movement of the axis to the center in Figs. 9b and 11b confirms an accelerated damped vibration.

It can be concluded from Figs. 10b and 12b that irregular spacing has stability effects on modes 2–4. For vibrations in mode 1, keeping the rubbing coefficients low is shown to be an effective way to damp the vibrations (Figs. 9b, 11b).

Conclusions

In this work, finite element modeling of the reamer was applied in order to study the vibration of the tool at low cutting speeds. The tool behavior was considered under a new model of external force application. The cutting and rubbing forces as external forces were applied as distributed forces on a variable engagement length of common reamers that are tapered with small angles. This assumption makes the simulation closer to the real reaming process, in comparison to point load assumption used in previous works.

The quasi-static reaming process formulation led to an eigenvalue problem with solutions that included oscillatory and unstable modes. Eigenvalue results that define oscillatory and unstable modes were compared for both concentrated and

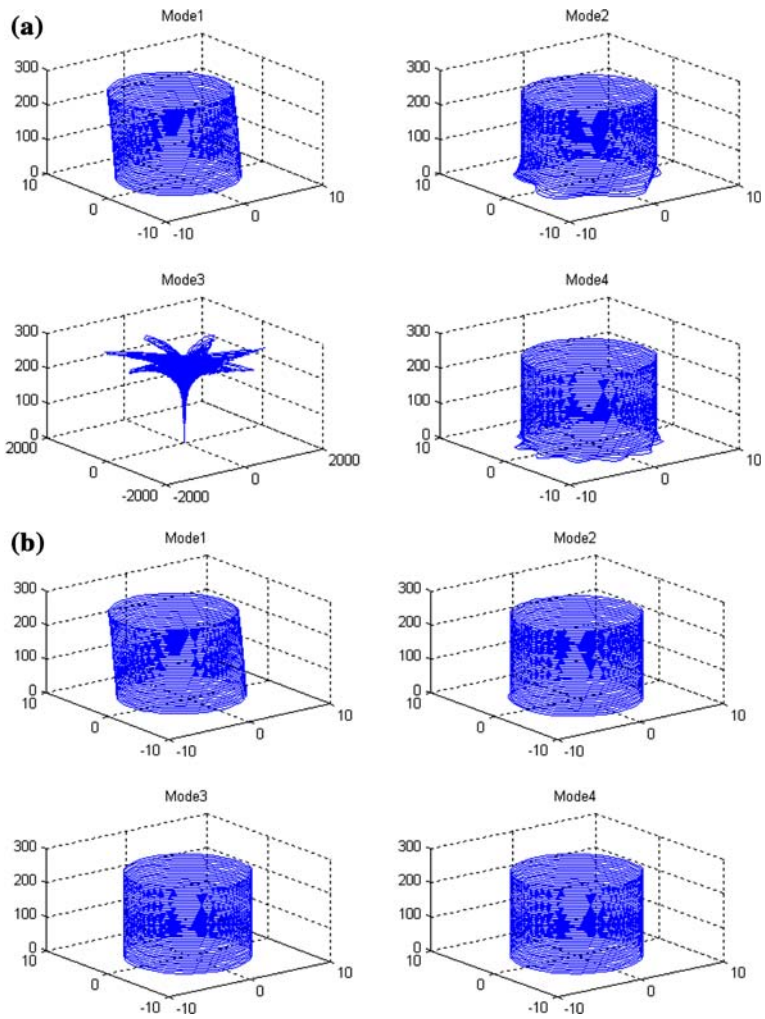

Fig. 12 3D hole profiles for the distributed force model on the variable engagement length for 16 elements ($k_r = 211$ N/mm, $\theta_r = 2$ degrees, $\alpha = \frac{\pi}{6}$). (**a**) Regular (**b**) Irregular spacing

distributed force models. It was shown that the concentrated force model in previous works yielded more incautious results than the distributed force model, which considered variable engagement length. Specifically, for cutting systems with lower rubbing coefficients, the difference between results of these two assumptions was more noticeable. In the concentrated force model, tool vibration is completely a damped vibration, while in the distributed force model, vibration starts as a damped vibration, but as the reamer advances, it tends to become periodic. For high rubbing coefficient systems, results of either concentrated or distributed force assumptions are very close.

Geometry modification of the reamer leading to more negative decaying rate or more stable conditions was investigated through uneven pitch spacing. For a six-flute reamer, irregular tooth spacing was considered by slight changes in pitch angle from the regular case. The irregular spacing proposed introduced a considerable damping into the system for modes of higher than one, leading to a perfect hole quality after the reaming process. The best combination of pitch angles leading to the most stable condition was proposed for a specific cutting condition. More accurate 2D and 3D hole profiles for irregular and regular spacing were presented through the distributed force model on variable engagement length of the reamer. It was observed that the geometry modification had effects on modes other than the first mode of vibration. For the first mode of vibration, lowering the rubbing coefficient was a proposed solution, the methods of which should be investigated in the future.

References

Bayly, P. V. (1997). Optimal 'White-Noise' spacing of reamer blades. In T. Bains & D. S. MacKenzie (Eds.), *Proceedings of the 1997 ASM International Non-Ferrous Processing and Technology Conference* (pp. 419–423). ASM International, Materials Park.

Bayly, P. V., Lamar, M. T., & Calvert, S. G. (2002). Low-frequency regenerative vibration and the formation of lobed holes in drilling. *Journal of Manufacturing Science and Engineering, 124*, 275–285.

Bayly, P. V., Metzler, S. A., Schaut, A. J., & Young, K. A. (2001b). Theory of torsional chatter in twist drills: Model, stability analysis and composition to test. *Journal of Manufacturing Science and Engineering, 123*, 552–561.

Bayly, P. V., Young, K. A., Calvert, S. D., & Halley, J. E. (2001a). Analysis of tool oscillation and hole roundness error in a Quasi-static model of reaming. *Journal of Manufacturing Science and Engineering, 123*, 387–396.

Bayly, P. V., Young, K. A., & Halley, J. E. (1998). Dynamic simulation of reaming: Theory, methods and application to the problem of lobed holes. *Dynamics, Acoustics and simulations, ASME publication DE, 98*, 245–252.

Budak, E., & Altintas, Y. (1993). Prediction of milling coefficients from orthogonal cutting data. *ASME Winter Annual Meeting, New Orleans, PED 64*, 453–459.

Budak, E., & Altintas, Y. (1995). Analytical prediction of stability lobes in milling. *CIRP Annals,* Jan 1995.

Cheung, Y. K., & Leung, A. Y. (1991). *Finite element methods in Dynamics*. Kluwer Academic.

Koenigsberger, F., & Tlusty, J. (1970). *Structres of machine tools*. Oxford: Pergamon Press.

Li, C.-J., Ulsoy, A. G., & Endres, W. J. (1998). The effect of the tool rotation on regenerative chatter in line boring. In R. P. S. Han, K. H. Lee, & A. C. J. Luo (Eds.), *Dynamics, Acoustics and simulations, ASME publication DE, 98*, 235–243.

Logan, D. L. (1999). *A first course in the finite element method using algor*. Thomson Engineering.

Metzler, S. A., Bayly, P. V., Young, K. A., & Halley, J. E. (1999). Analysis and simulation of radial chatter in drilling and reaming. *Proceedings of ASME DETC'99,(CD)*, Paper No. V1B8059.

Sakuma, K., & Kiyota, H. (1968a). Hole accuracy with carbide-tipped reamers: 1st report. *Bulletin of the Japan Society of Precision Engineering, 19*, 89–95.

Sakuma, K., & Kiyota, H. (1968b). Hole accuracy with carbide-tipped reamers: 2nd report. *Bulletin of the Japan Society of Precision Engineering, 20*, 103–108.

Sridhar, R., Hohn, R. E., & Long, G. W. (1968a). A general formulation of the milling processing equation: Contribution for machine tool chatter research 5. *ASME Journal of Engineering for Industry, 90*, 317–324.

Sridhar, R., Hohn, R. E., & Long, G. W. (1968b). A stability algorithm for the general milling process. *Trans. ASME Journal of Engineering for Industry, 90*, 330–334.

Tlusty, J. (1985). Machine dynamics. In R. I. King (Ed.), *Handbook of high speed machining technology*. New York: Chapman & Hall.

Tlusty, J., & Polacek, M. (1963). The stability of machine tools against self-excited vibrations in machining. *ASME International Research in Production Engineering,* 465–474.

Tobias, S. A. (1965). *Machine tool vibration*. Bishopbriggs, UK: Blackie and Son.

Towfighian, S. (2006). *Finite element modeling of low speed reaming in the application of femoral canal preparation for intramedullary nailing*. M.A.Sc. thesis, Ryerson University, Toronto, Canada.

Varterasian, J. H. (1974). *Society of manufacturing engineers technical Paper MR74-144*, pp. 1–15.